Pergamon

0022-4073(94)E0002-N

J. Quant. Spectrosc. Radiat. Transfer Vol. 51, No. 5, pp. 759–778, 1994
Elsevier Science Ltd
Printed in Great Britain
0022-4073/94 $7.00 + 0.00

LIGHT SCATTERING BY POLYDISPERSE, ROTATIONALLY SYMMETRIC NONSPHERICAL PARTICLES: LINEAR POLARIZATION

MICHAEL I. MISHCHENKO†‡ and LARRY D. TRAVIS§

†NASA Goddard Institute for Space Studies and Hughes STX Corporation, 2880 Broadway, New York, NY 10025, and §NASA Goddard Institute for Space Studies, New York, NY 10025, U.S.A.

(Received 23 July 1993)

Abstract—Since most solid particles in the Earth and planetary atmospheres have irregular shapes, quantifying the effects of particle nonsphericity on the results of remote sensing of the atmosphere is an important problem. In this paper, we perform a general theoretical survey of linear polarization of light scattered by polydisperse, randomly oriented, rotationally symmetric particles of size comparable to the wavelength of radiation. Our paper deals with polydispersions of nonspherical particles because (1) averaging light-scattering characteristics over sizes provides more realistic modeling of natural particle ensembles and (2) comparisons of scattering properties of particles of a single size are usually meaningless because of the complicated interference structure and high-frequency ripple of monodisperse scattering patterns. In our computations, we use the T-matrix approach, as extended recently to randomly oriented particles by Mishchenko [*J. Opt. Soc. Amer. A* **8,** 871 (1991)]. Following Hansen and Travis [*Space Sic. Rev.* **16,** 527 (1974)], we assume that the scattering properties of polydisperse particles depend primarily on only the effective size parameter and effective variance of the size distribution, the particular shape of the distribution being of minor importance. Therefore, to describe the dispersion of particle sizes in the ensemble, we employ a convenient power law distribution of particle equivalent-sphere size parameters. Size-averaged light-scattering characteristics are calculated by numerically integrating monodisperse quantities using a Gaussian quadrature formula. The results of extensive numerical calculations for particles of different shape and refractive index are presented in the form of color contour diagrams of linear polarization as a function of scattering angle and effective equivalent-sphere size parameter. The influence of particle size distribution, shape, and refractive index on the polarization patterns is examined in detail and implications for polarimetric remote sensing of nonspherical aerosols are discussed. The diagrams displayed include calculations for over 150,000 different monodisperse particles in random orientation with equivalent-sphere size parameters up to 30 and may be used to interpret results of laboratory measurements and remote observations of light scattering by small particles.

1. INTRODUCTION

Most solid particles in terrestrial and planetary atmospheres are nonspherical and of course are also distributed over some size range. Therefore, the scattering of radiation by polydisperse nonspherical particles is a subject of interest in many areas of atmospheric science and remote sensing.[1–9] Until recently, the numerical methods for computing light scattering by randomly oriented nonspherical particles were very time-consuming. As a result, even the most detailed analyses of nonspherical scattering were based on studying only a few tens[10] or hundreds[11,12] of different nonspherical particles in random orientation, and computations for polydisperse randomly oriented particles were extremely scarce.[13–15]

Recently, Mishchenko[16,17] has developed a very efficient method for computing light scattering by randomly oriented rotationally symmetric particles of size comparable to the wavelength of radiation. This method is based on the T-matrix approach[18–20] and involves analytical rather than

‡To whom all correspondence should be addressed. E-mail: crmim@nasagiss.giss.nasa.gov.

numerical averaging of scattering characteristics over particle orientations. With the development of this method, computations for hundreds of thousands of different nonspherical particles in random orientation have become possible even on moderate computers, which makes this method especially suitable for computing light scattering by realistic polydisperse models of nonspherical particles.[21,22] Wauben[23] has performed direct comparisons of CPU times for Mishchenko's method and that of Kuik et al[15] by calculating the same models on the same computer. Kuik et al use an improved version of the T-matrix code by Barber and Hill[19] and employ straightforward numerical averaging over particle orientations in calculations for randomly oriented particles. The timing tests for Models 1–3 of Kuik et al have shown that Mishchenko's method is faster than that of Kuik et al by a factor of several tens. Also, timing tests reported in Refs. 11, 15 and 24 imply that for randomly oriented rotationally symmetric particles, Mishchenko's method is at least several orders of magnitude faster than Asano and Yamamoto's solution for spheroids[10,25,26] and many orders of magnitude faster than the discrete dipole approximation (DDA)[24] and volume integral equation formulation (VIEF).[27] Based on a detailed analysis of CPU-time requirements for the VIEF, Kuik[11] concludes that, at present, that method is not really suitable for accurate light scattering computations for ensembles of randomly oriented nonspherical particles. Apparently, this is true for the DDA as well. Also, the data published in Ref. 24 raise a question regarding the ability of the DDA to accurately calculate the elements of the scattering matrix for particles with size parameters greater than roughly 5–10. For example, DDA calculations of the phase function for a spherical particle having the size parameter 10 and index of refraction $1.33 + 0.01i$ and represented as an array of as many as 137,376 dipoles still show errors exceeding 20%.

In this paper, we use the Mishchenko method to perform a general survey of the linear polarization of light scattered by polydisperse, randomly oriented, rotationally symmetric particles of size comparable to a wavelength. Our survey is analogous to that presented by Hansen and Travis[28] for Mie scattering, albeit with some computational limitations on the maximum particle size. The principal aim of this survey is twofold. First, we demonstrate how the linear polarization depends on parameters of particle size distribution and particle shape and refractive index. Second, we examine how particle nonsphericity may influence the results of particle size distribution and refractive index retrievals from polarimetric remote measurements of scattered light.

The most significant difference of our survey from previous papers on nonspherical scattering is that we extensively study light scattering by size distributions of nonspherical particles rather than by particles of a single size. Comparing light scattering properties of monodisperse particles with size parameters greater than roughly 3 is usually meaningless because of the complicated interference structure and high-frequency ripple of scattering patterns.[28,29] As was noticed by Wiscombe and Mugnai[30] on the basis of their extensive calculations for monodisperse Chebyshev particles,[12] the spherical and nonspherical curves for a single particle size very often form a tangle of lines with no clear message. Averaging over sizes, besides providing more realistic modeling of natural ensembles of scattering particles, removes the interference structure and ripple and allows one to draw general conclusions about the effects of nonsphericity on light scattering.

In this paper we focus our attention on linear polarization, based on the following rationale. First, although intensity is the most commonly measured quantity, linear polarization has the advantage of being obtainable from a relative measurement and, therefore, can be measured with significantly higher accuracy than intensity.[28] Measurement errors are usually smaller than the characteristic features in the variation of the scattered light polarization with particle size and scattering angle. As a result, linear polarization is potentially a valuable source of information about the scattering particles. This was convincingly demonstrated, e.g., by Hansen and Hovenier,[31] Kawabata et al,[32] and Santer et al[33] who used polarimetry as a sensitive remote sensing technique for determining the size and refractive index of aerosol particles in the Earth and Venus atmospheres. Second, spherical/nonspherical differences are much more pronounced in polarization than in intensity. In particular, even the sign of polarization can be different for volume- or surface-equivalent spheres and nonspherical particles of the same refractive index. Third, quantifying effects of particle nonsphericity on measured polarization can be an important task in interpreting polarimetric data from the Galileo Orbiter Photopolarimeter/Radiometer,[34] Earth Observing Scanning Polarimeter (EOSP),[35,36] and Polarization and Directionality of the Earth's Reflectances instrument (POLDER).[37] Note that the EOSP was specifically designed to provide

accurate quantitative information on radiative properties of tropospheric aerosols in the Earth atmosphere which may be an important source of climate forcing.[36] Such information would be hardly obtainable with purely photometric techniques.

The plan of our paper is as follows. In the next section, we introduce basic definitions and conventions and present results of extensive calculations of linear polarization for size distributions of nonspherical particles. In Sec. 3, we use these numerical data to examine the effects of particle size distribution, shape, and refractive index on the patterns of linear polarization, and to draw the corresponding implications for polarimetric remote sensing of nonspherical aerosols. In the concluding section, we summarize the principal results of the paper.

2. CALCULATIONS

2.1. Linear polarization

In the standard $\{I, Q, U, V\}$ representation of polarization, the scattering matrix for randomly oriented rotationally symmetric particles has the form[38]

$$\boldsymbol{F}(\vartheta) = \begin{bmatrix} F_{11}(\vartheta) & F_{22}(\vartheta) & 0 & 0 \\ F_{12}(\vartheta) & F_{22}(\vartheta) & 0 & 0 \\ 0 & 0 & F_{33}(\vartheta) & F_{34}(\vartheta) \\ 0 & 0 & -F_{34}(\vartheta) & F_{44}(\vartheta) \end{bmatrix}, \tag{1}$$

where ϑ is the scattering angle. The degree of linear polarization for single scattering of unpolarized incident light $P(\vartheta)$ is defined as[28]

$$P(\vartheta) = -100F_{12}(\vartheta)/F_{11}(\vartheta). \tag{2}$$

To calculate numerically the elements of the scattering matrix for polydispersions of randomly oriented, rotationally symmetric particles, we use the method described in detail by Mishchenko.[17,21] For all the calculations reported below, the absolute accuracy of computing F_{11} and F_{12} is expected to be (much) better than 0.001.

2.2. Particle shape

Three families of nonspherical, rotationally symmetric shapes have been extensively used in light scattering computations: spheroids,[10,11,13–16,21,22,26,39–45] finite cylinders,[11] and so-called Chebyshev particles.[3,12,30] Of these families, spheroidal particles have the following important advantages. The shape of a spheroid is specified by only one parameter, the aspect ratio, along with the designation of either prolate or oblate. By varying this single parameter, a wide variety of particle shapes ranging from needles to plates can be modeled. To specify the shape of a Chebyshev particle, two parameters are required and, because of slow convergence of T-matrix computations for Chebyshev particles, only a relatively modest degree of nonsphericity ("surface roughness" of nearly spherically shaped particles) can be modeled.[3,12] Second, unlike finite cylinders, the entire surface of spheroids is smooth, thus allowing convergent T-matrix computations for relatively larger size parameters and aspect ratios. With these considerations in mind, we have selected the family of spheroidal shapes as the primary for this survey. However, in Sec. 3.3 a limited volume of computations for Chebyshev particles will be used to briefly discuss the effects of partial concavity of particle shape.

The shape of a spheroid in the spherical coordinate system is governed by the equation

$$r(\theta, \phi) = a\left[\sin^2\theta + \frac{a^2}{b^2}\cos^2\theta\right]^{-1/2}, \tag{3}$$

where θ is the zenith angle, ϕ is the azimuth angle, b is the rotational (vertical) semi-axis, and a is the horizontal semi-axis. The aspect ratio of the spheroid ϵ (the ratio of the largest to smallest dimensions) is defined as

$$\epsilon = \begin{cases} b/a & \text{for prolate spheroids,} \\ a/b & \text{for oblate spheroids.} \end{cases} \tag{4}$$

2.3. Parametrization of particle size

Any meaningful comparison of light scattering properties of particles of different shape requires the specification of an "equivalent" particle size. Different definitions of particle equivalence have been adopted by various investigators, the most popular being the definitions in terms of equal volume, equal surface area, and equal averaged projected area (for randomly oriented convex particles, the last two definitions are identical[46]). The definition in terms of equal volume seems to be the best for particles much smaller than the wavelength of radiation, since in this limit scattering depends primarily on particle volume rather than surface or projected area.[29,38] The definition in terms of equal averaged projected area seems to be more relevant in the case of particles much greater than the wavelength because in this case the diffraction intensity peak and extinction cross section depend primarily on the averaged projected area. In this paper, our interest is in particles of size comparable to the wavelength, in which case all the definitions can give poor results,[21] and the choice of definition becomes rather arbitrary. However, we have chosen the definition of particle equivalence in terms of equal averaged projected area because this definition seems to be more relevant in a greater range of practical problems and is key in the definition of the effective radius and effective variance of the particle size distribution [Eqs. (8)–(10)]. As a consequence of this choice, the main size characteristic of a spheroidal particle in our paper is the radius of the sphere that has the cross-sectional area equal to the averaged projected area of randomly oriented spheroids, or, equivalently, the radius of the equal-surface-area sphere given by

$$r = \frac{1}{2}\left[2a^2 + 2ab\frac{\arcsin e}{e}\right]^{1/2} \tag{5}$$

for prolate spheroids and by

$$r = \frac{1}{2}\left[2a^2 + \frac{b^2}{e}\ln\left(\frac{1+e}{1-e}\right)\right]^{1/2} \tag{6}$$

for oblate spheroids, with e being defined as

$$e = \frac{1}{\epsilon}\sqrt{\epsilon^2 - 1}. \tag{7}$$

Also we define the particle equivalent-sphere size parameter x as $x = 2\pi r/\lambda$, where λ is the wavelength of light.

2.4. Size distribution

Hansen and Travis[28] (see also Hansen and Hovenier[31] and Lacis et al[47]) have shown that the scattering properties of most physically plausible size distributions of spherical particles depend primarily on only two characteristics of the distribution, the particular shape of the distribution being of minor importance. These two characteristics are the effective size parameter x_{eff} and effective variance v_{eff} defined as

$$x_{\text{eff}} = \frac{1}{G}\int_0^\infty x\pi x^2 n(x)\,\mathrm{d}x, \tag{8}$$

$$v_{\text{eff}} = \frac{1}{Gx_{\text{eff}}^2}\int_0^\infty (x - x_{\text{eff}})^2\pi x^2 n(x)\,\mathrm{d}x, \tag{9}$$

where $n(x)\,\mathrm{d}x$ is the fraction of particles with size parameters from x to $x + \mathrm{d}x$, and G is given by

$$G = \int_0^\infty \pi x^2 n(x)\,\mathrm{d}x. \tag{10}$$

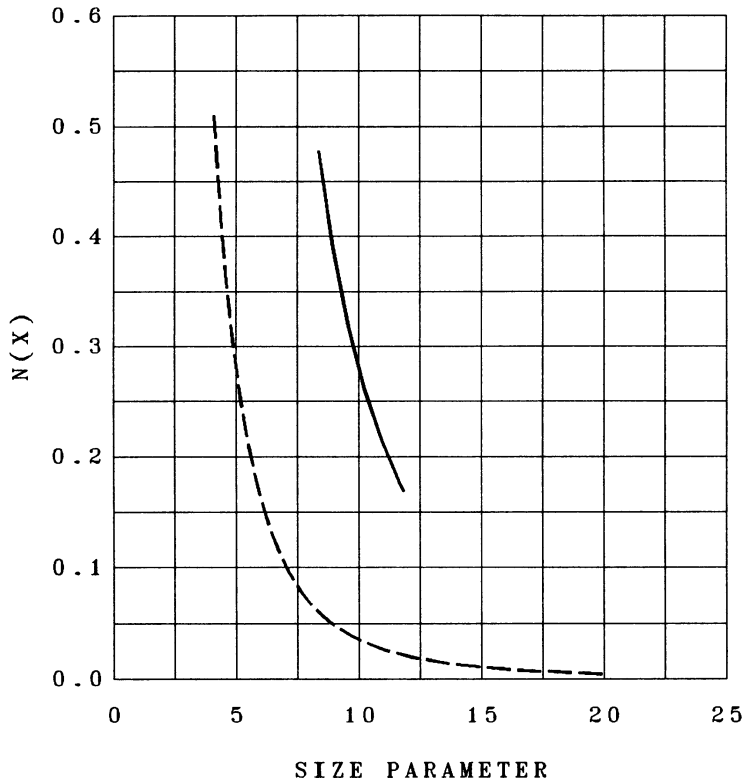

Fig. 1. (—) shows a narrow power law size distribution with $x_1 = 8.3662$ and $x_2 = 11.8338$ corresponding to $x_{\text{eff}} = 10$ and $v_{\text{eff}} = 0.01$. (– – –) shows a wider distribution with $x_1 = 4.0972$ and $x_2 = 19.9028\,\mu$m corresponding to the same $x_{\text{eff}} = 10$ but $v_{\text{eff}} = 0.2$.

In this paper, we assume that the same is true for randomly oriented nonspherical particles, provided that the sphere size parameter is replaced by the equal-projected-area-sphere size parameter, and use the so-called power law size distribution[28] $n(x) \propto x^{-m}$, $x \in [x_1, x_2]$. Following Ref. 28, we use in this paper the exponent $m = 3$. Thus we have

$$n(x) = \begin{cases} \dfrac{2x_1^2 x_2^2}{x_2^2 - x_1^2} x^{-3}, & \text{for } x_1 \leqslant x \leqslant x_2, \\ 0, & \text{otherwise} \end{cases} \tag{11}$$

(see Fig. 1). This distribution has the following three important advantages. (1) Unlike, e.g., gamma and log normal distributions,[28] for the power law distribution the lower and upper limits x_1 and x_2 are explicit parameters and are fixed rather than determined depending on the required numerical accuracy of the computations. As a result, checking convergence of the computations over these parameters is avoided. (2) For a given effective size parameter and effective variance and some reasonable accuracy requirement on the computations, the power law distribution has much smaller upper limit of particle size parameters x_2 than the gamma and log normal distributions,[28] thus allowing convergent T-matrix computations for greater x_{eff} and v_{eff} and a wider range of particle aspect ratios. (3) The power law distribution reasonably well reproduces many size distributions determined for natural particle ensembles and is widely used in atmospheric science (e.g., Refs. 48 and 49).

In this paper, we use x_{eff} and v_{eff} rather than x_1 and x_2 as the primary formal parameters of the power law size distribution. For a given value of v_{eff}, x_1 and x_2 are proportional to x_{eff}. Denoting $q_1 = x_1/x_{\text{eff}}$ and $q_2 = x_2/x_{\text{eff}}$ we determine the coefficients q_1 and q_2 from the following system of two

(nonlinear) equations:

$$\frac{(q_2 - q_1)}{\ln(q_2/q_1)} = 1, \tag{12}$$

$$q_2 + q_1 = 2(v_{\text{eff}} + 1). \tag{13}$$

The values of the coefficients q_1 and q_2 for some values of the effective variance are given in Table 1.

2.5. Refractive indices

In this paper, most of calculations are reported for the refractive index $1.5 + 0.02i$ typical of mineral dust aerosols in the visible and near infrared spectral regions.[50,51] This refractive index was also used by Wiscombe and Mugnai[12] in their study of light scattering by Chebyshev particles. To investigate the effects of refractive index on nonspherical linear polarization, we also use several other real and imaginary refractive indices ranging from 1.3 to 1.75 and from 0.003 to 0.3, respectively.

2.6. Color contour diagrams of linear polarization

To display the substantial volume of numerical results in an efficient and yet comprehensible form, we use color contour diagrams of linear polarization as a function of the scattering angle ϑ (horizontal axis) and effective size parameter x_{eff} (vertical axis) (Figs. 2–9). The contour levels used throughout are illustrated by the color bar displayed in Fig. 2. Orange-red colors correspond to positive linear polarization (i.e., the larger of the orthogonal intensity components is that perpendicular to the scattering plane) and blue-violet colors represent negative values. In most plots, contour lines for 0, ± 10, ± 20, ± 40, ± 60, ± 80, and $\pm 95\%$ polarization are superposed on the color display as illustrated in the color bar. We did not label the contours because the use of colors makes the contour diagrams easily readable even without labels. In some cases putting contours was meaningless because of too rapid a change of polarization within a small range of scattering angles and size parameters. In those cases, color images can be quantified by using the color bar.

To create polydisperse polarization diagrams, we performed T-matrix computations for effective size parameters x_{eff} from 0.2 to 15 with step size $\Delta x_{\text{eff}} = 0.2$. T-matrix computations cannot be performed for exactly zero size parameter. However, with $x_{\text{eff}} \to 0$ polarization does not become peculiar but rather evenly tends to the Rayleigh limit.[29,38] As a result, we have found that extrapolation of the computations for $x_{\text{eff}} \in [0.2, 15]$ to $x_{\text{eff}} = 0$ gives excellent results.

We present, in Figs. 2–9, a series of panels of these color contour diagrams which have been selected from a much more extensive set of computations in order to appropriately illustrate the dependence of the general features of the linear polarization on the parameters of the particle size distribution and particle shape and refractive index. In the following section, we discuss the apparent characteristics and our observations regarding the implications for the appropriate treatment of situations involving nonspherical particles. Because of the large volume of the numerical data displayed, we focus our attention on the most general trends and characteristics. A detailed analysis of particular features in each of the polarization diagrams can easily be performed by any interested reader.

Table 1. Coefficients q_1 and q_2 for some values of the effective variance v_{eff}.

v_{eff}	q_1	q_2
0	1	1
0.01	0.83662	1.18338
0.03	0.72910	1.33090
0.05	0.66076	1.43924
0.1	0.54677	1.65324
0.2	0.40972	1.99028

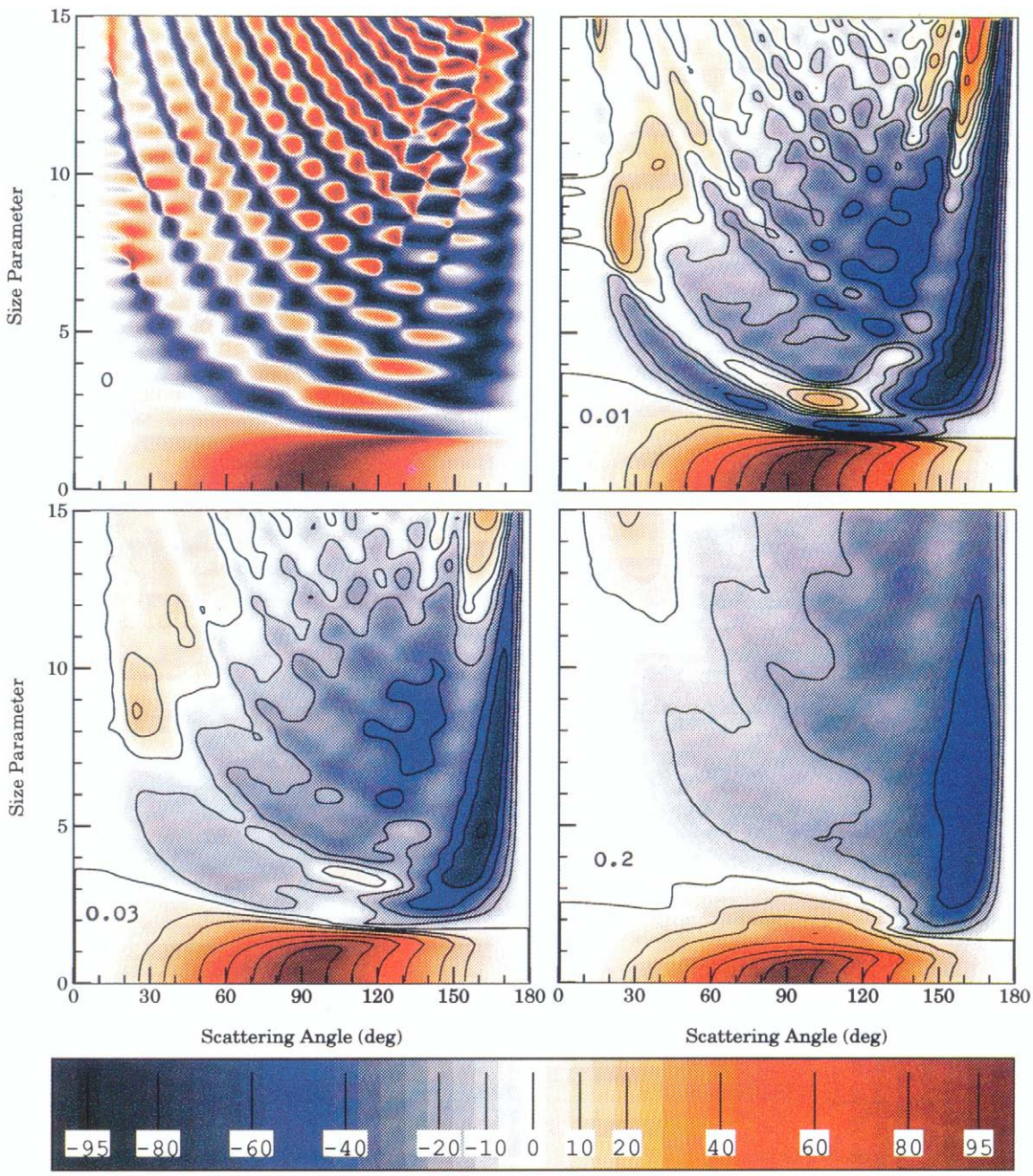

Fig. 2. This figure demonstrates the effects of increasing width of the particle size distribution and shows color contour diagrams of linear polarization as a function of the scattering angle ϑ (horizontal axes) and effective size parameter x_{eff} (vertical axes) for the power law size distribution of spherical particles with the index of refraction $1.5 + 0.02i$. Labels show values of the effective variance v_{eff}. The value $v_{\mathrm{eff}} = 0$ corresponds to monodisperse particles. The color bar shows the set of contour levels used throughout this paper.

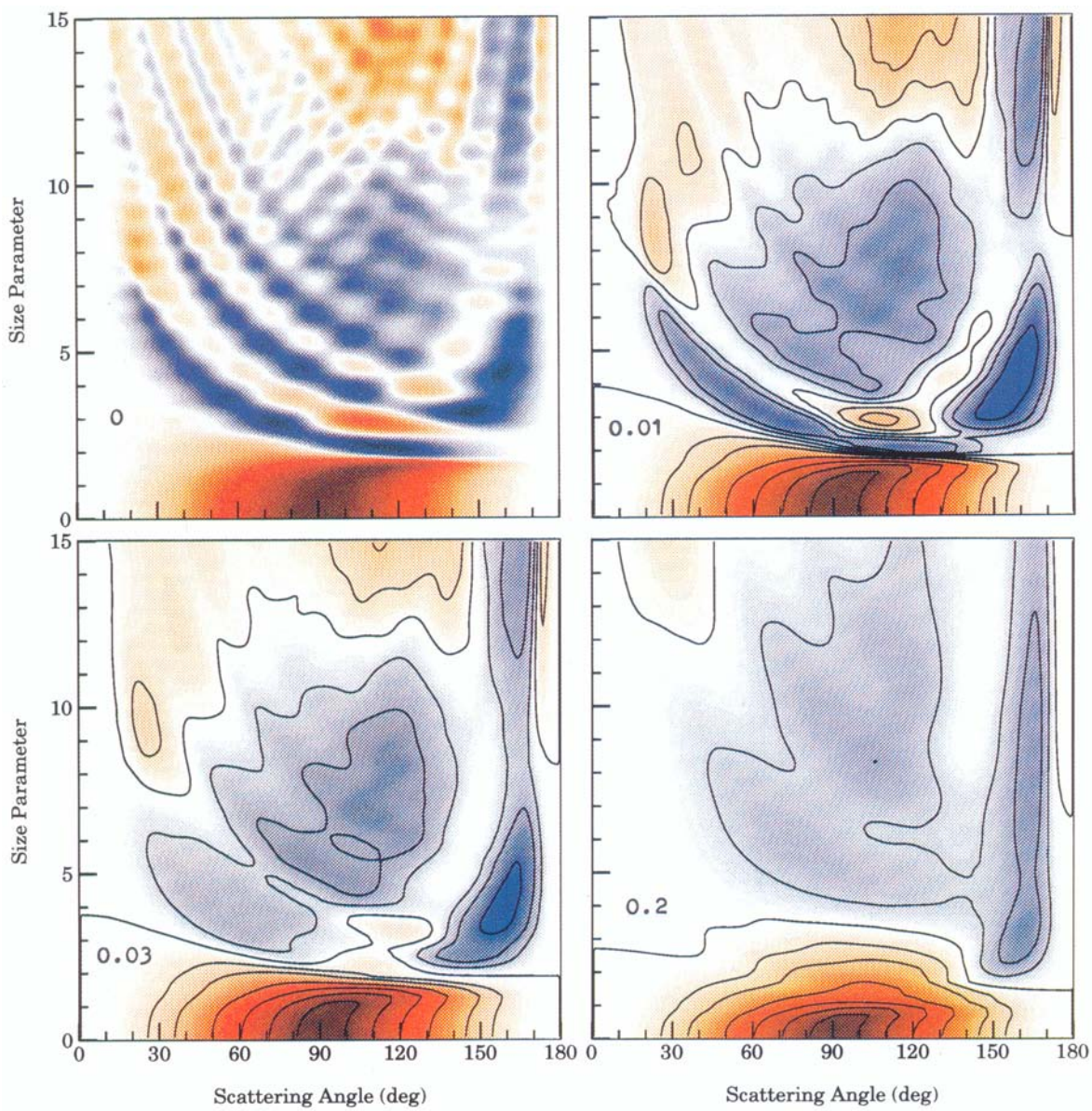

Fig. 3. As in Fig. 2, but for randomly oriented oblate spheroids with the aspect ratio $\epsilon = 1.4$.

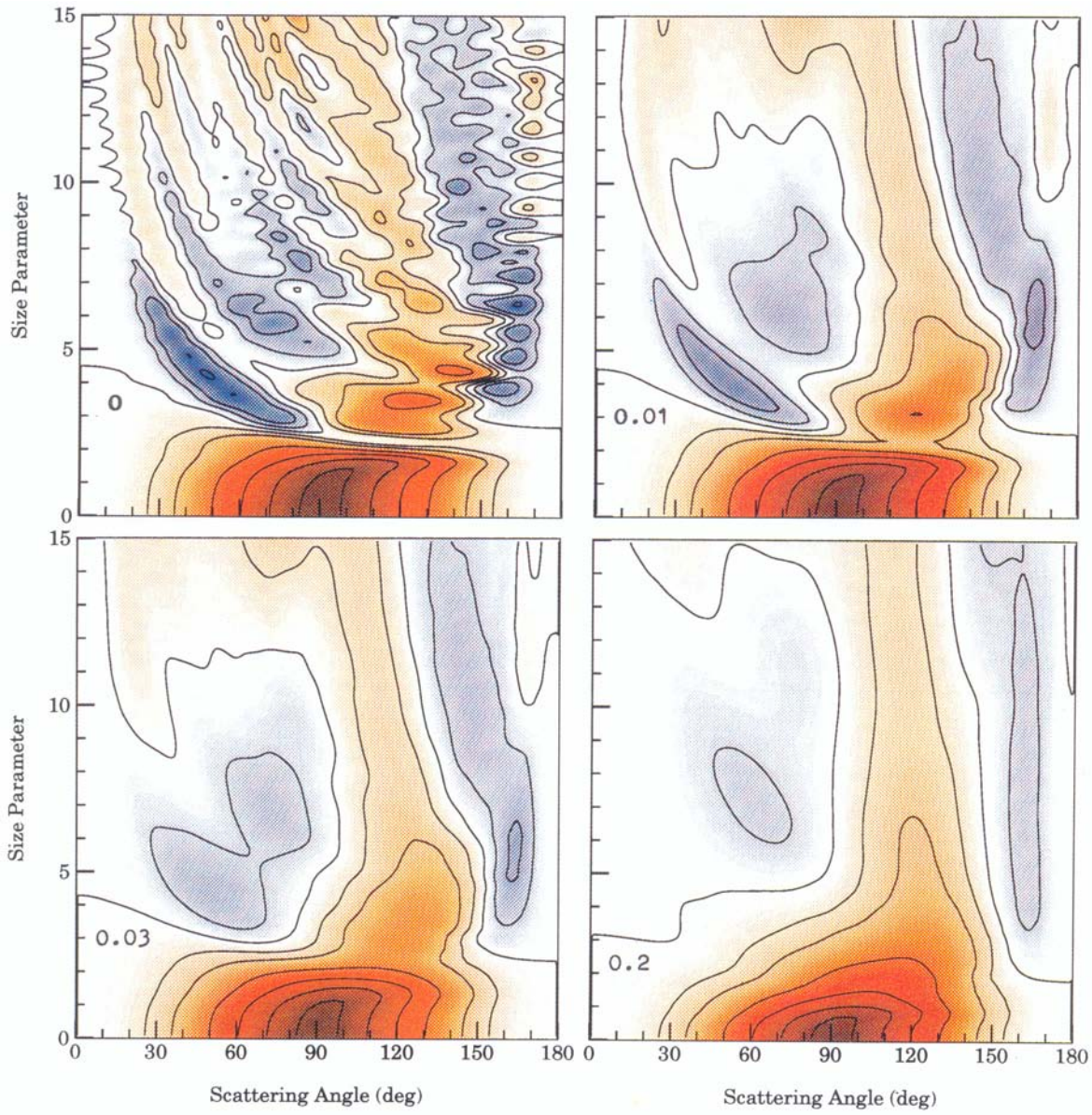

Fig. 4. As in Fig. 2, but for randomly oriented oblate spheroids with the aspect ratio $\epsilon = 2$.

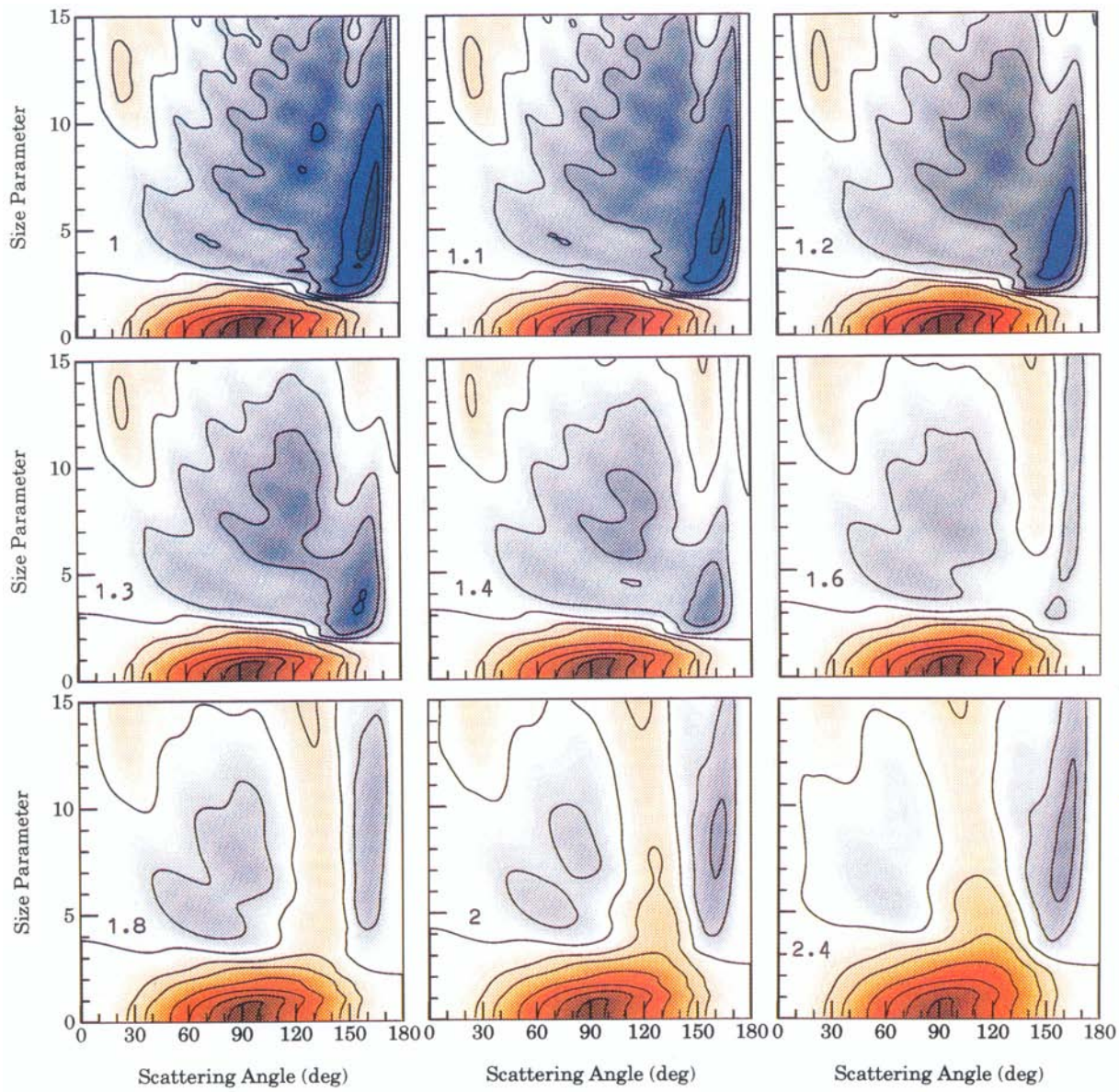

Fig. 5. This figure demonstrates the effects of increasing particle aspect ratio and shows color contour diagrams of linear polarization for polydisperse, randomly oriented prolate spheroids with the index of refraction $1.5 + 0.02i$ and effective variance $v_{\mathrm{eff}} = 0.1$. Labels show the values of the aspect ratio ϵ.

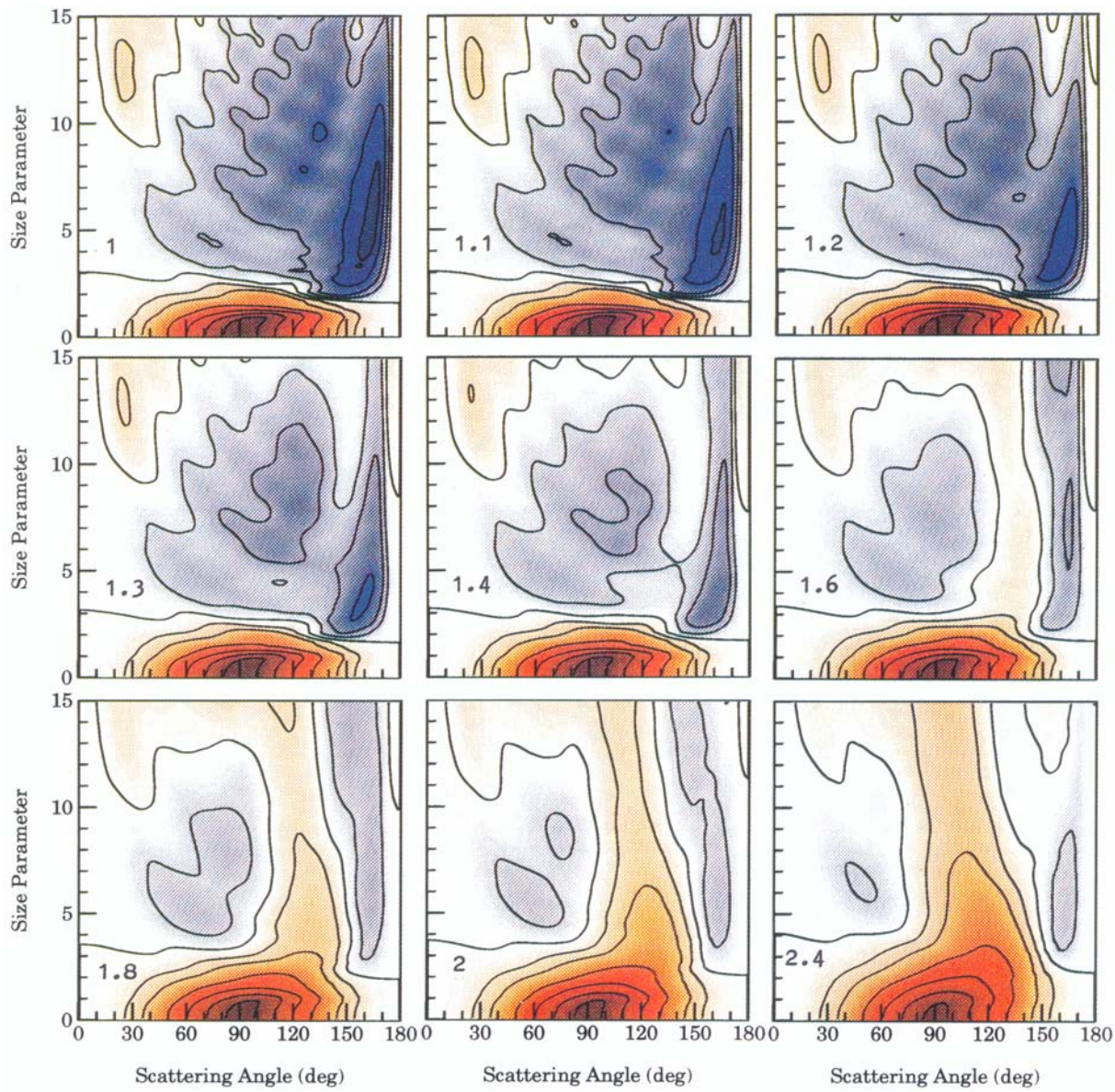

Fig. 6. As in Fig. 5, but for oblate spheroids.

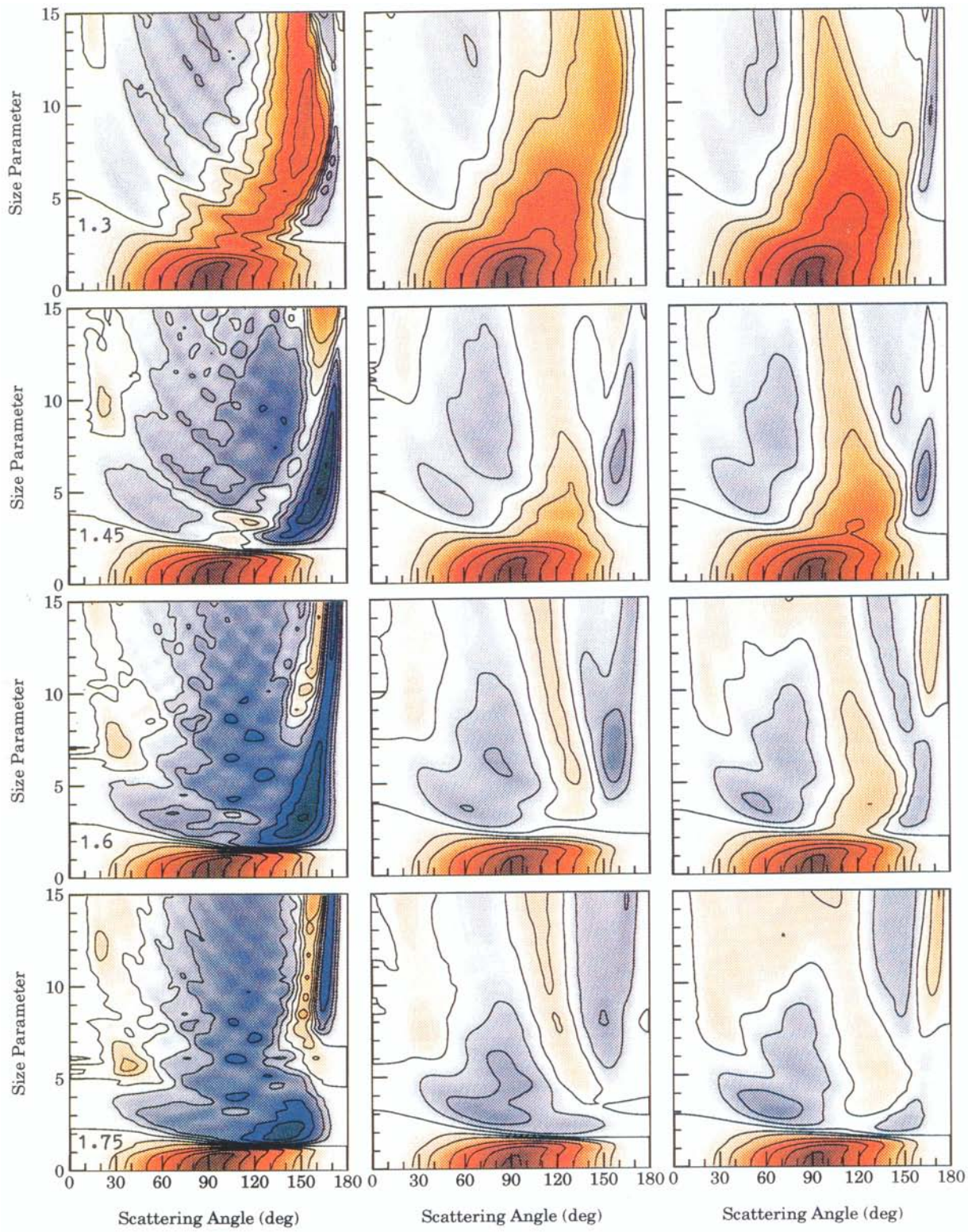

Fig. 7. This figure demonstrates the effects of the real part of the refractive index and shows color contour diagrams of linear polarization for polydisperse spheres (left column) and equivalent randomly oriented prolate (middle column) and oblate (right column) spheroids with the aspect ratio $\epsilon = 2$. The real refractive indices are 1.3, 1.45, 1.6, and 1.75, as shown by the labels. The imaginary refractive index is 0.003, and the effective variance is $v_{\mathrm{eff}} = 0.03$.

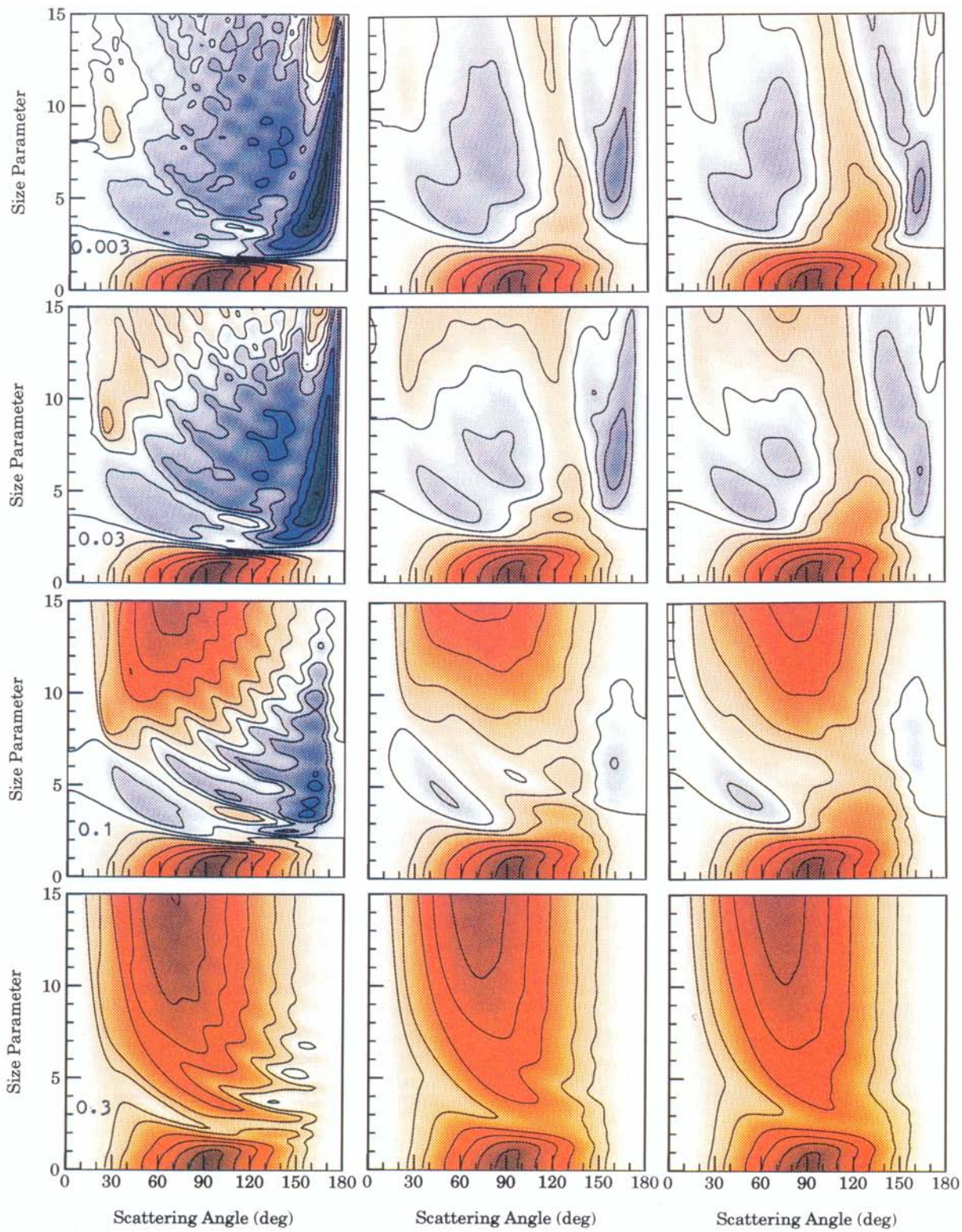

Fig. 8. This figure demonstrates the effects of the imaginary part of the refractive index and shows color contour diagrams of linear polarization for polydisperse spheres (left column) and equivalent randomly oriented prolate (middle column) and oblate (right column) spheroids with the aspect ratio $\epsilon = 2$. The imaginary refractive indices are 0.003, 0.03, 0.1, and 0.3, as shown by the labels. The real refractive index is 1.5, and the effective variance is $v_{\mathrm{eff}} = 0.03$.

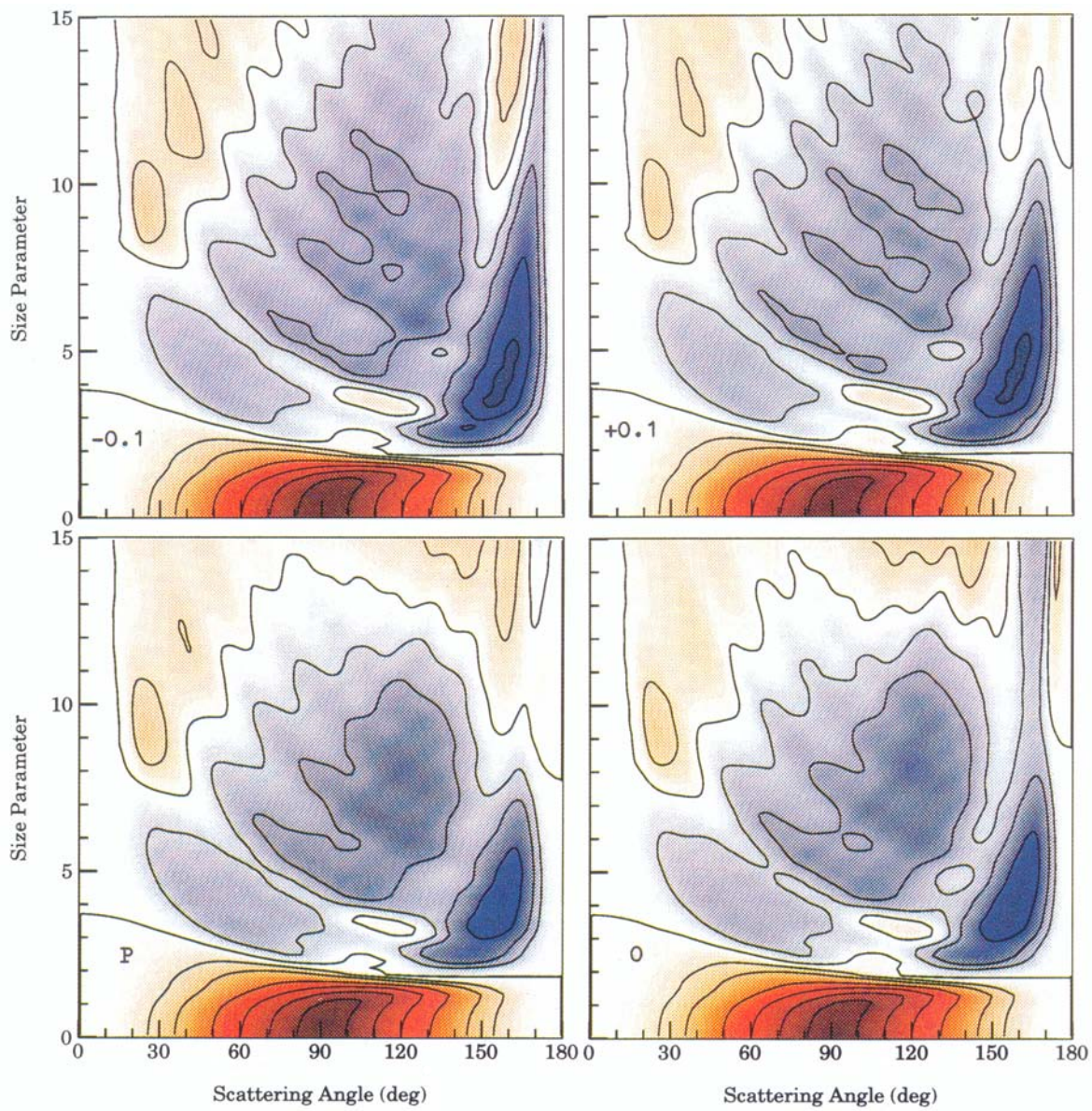

Fig. 9. This figure demonstrates the effects of partial concavity of nonspherical particles and shows color contour diagrams of linear polarization for polydisperse, randomly oriented Chebyshev particles and spheroids with $v_{\mathrm{eff}} = 0.03$ and index of refraction $1.5 + 0.02i$. The labels $+1$ and -1 indicate Chebyshev particles with $n = 4$ and $\xi = +0.1$ and $\xi = -0.1$, respectively. Prolate and oblate spheroids with the aspect ratio $\epsilon = 1.3$ are indicated by letters "P" and "O", respectively. The vertical axes show the values of the effective equal-surface-area-sphere size parameter.

3. DISCUSSION

3.1. *Effects of size distribution*

Figures 2–4 show that, with the exception of the region of Rayleigh scattering ($x_{\text{eff}} \lesssim 1$), the polarization diagrams for particles with $v_{\text{eff}} = 0$ are essentially patterns of local maxima and minima which results from interference phenomena for particles of a single size[28] and make comparison of polarization characteristics for different monodisperse particles both problematic and not very relevant for consideration of realistic particle populations in nature. This interference structure is especially pronounced for spheres (Fig. 2) and becomes weaker with increasing particle nonsphericity as represented by larger aspect ratios (Figs. 3 and 4).

It should be noted that, because of this interference structure, the generation of polarization diagrams for $v_{\text{eff}} = 0$ requires special care, even for spheroidal particles. To create the monodisperse plots in Figs. 2–4, we performed calculations with step sizes $\Delta\vartheta = 0.5°$ and $\Delta x = 0.0025$. Using the same step sizes, we calculated the polarization for randomly oriented monodisperse prolate spheroids with the refractive index 1.44 and aspect ratio $\epsilon = 2$ in order to compare our computations with those previously published by Asano and Sato.[10] Our results are displayed in Fig. 10, where for this figure only, the vertical axis shows the values of the equal-volume-sphere size parameter. Comparison of Fig. 10 with Fig. 11 of Asano and Sato[10] reveals substantial differences which most likely result from step sizes too large in both scattering angle and size parameter used by those authors.[52]

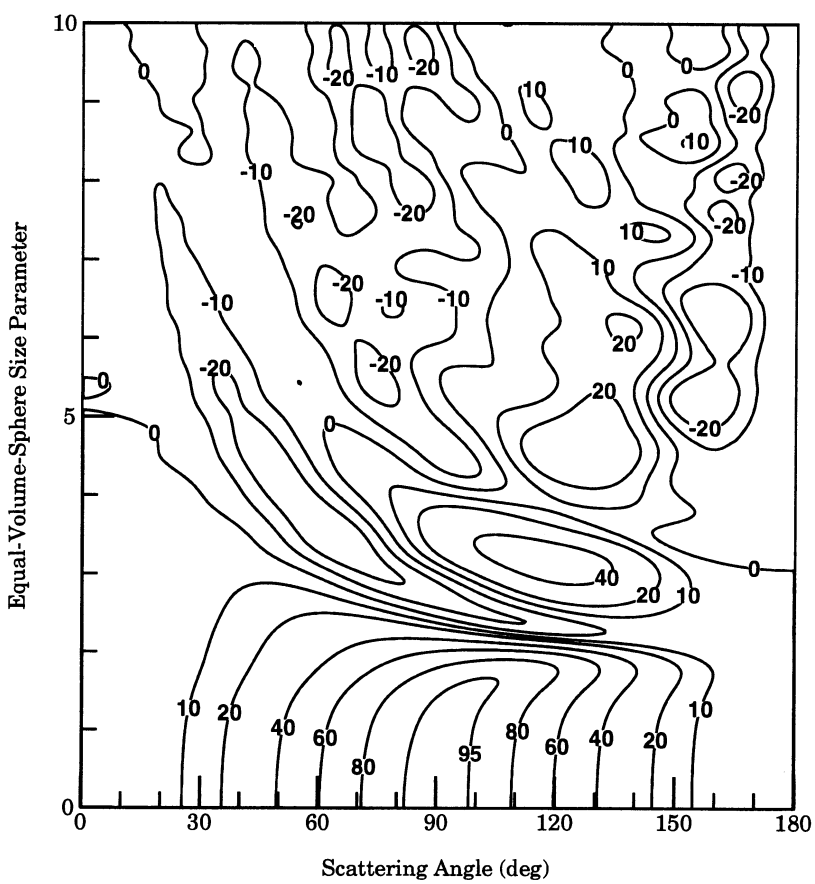

Fig. 10. Contour diagram of linear polarization as a function of the scattering angle and equal-volume-sphere size parameter for monodisperse, randomly oriented prolate spheroids with the index of refraction 1.44 and aspect ratio $\epsilon = 2$ (cf. Fig. 11 of Asano and Sato[10]).

Figures 2–4 show that, irrespective of the shape of scattering particles, the general effect of the dispersion of particle sizes in the distribution is to smooth out most of the interference effects and reduce the magnitude of the polarization features. With increasing v_{eff}, maxima are smoothed out, minima are filled in, and corners in contour lines are rounded off. An additional effect of increasing v_{eff} is a depression to smaller size parameters of the region of maximum polarization corresponding to Rayleigh scattering. All these effects of broadening the size distribution are easy to understand qualitatively in terms of taking weighted averages along vertical lines of increasing length in polarization diagrams for monodisperse particles.[28]

3.2. *Effects of particle shape and refractive index*

As was noted above, one of the effects of increasing particle aspect ratio is to weaken the interference structure and to make the linear polarization more neutral. For polydisperse particles, this smoothing effect of nonsphericity is superposed on the effect of size distribution, further reducing the magnitude of polarization and making contour lines even smoother. Since this effect of particle shape is qualitatively similar to that of increasing width of the size distribution, one might expect in some cases (especially when the volume of experimental data is limited) an overestimation of the retrieved width of the size distribution if the Mie theory is used to represent the light scattering by nearly spherically shaped particles. Figures 2–4 also show that the dependence of the polarization patterns on the width of the size distribution becomes much weaker for larger values of the aspect ratio ϵ. This means that in practical computations for polydisperse highly irregular particles, one may use a smaller value for the effective variance than that corresponding to the actual distribution and still adequately represent the scattering characteristics in contrast to the situation for spherical or nearly spherical particles and thereby substantially reduce the CPU time requirements.

On the other hand, our calculations shown in Figs. 2–7 clearly demonstrate that the total effect of particle shape on polarization is not equivalent to the effect of size distribution, especially for bigger particles. In other words, particle nonsphericity very often changes polarization in such a way that cannot be reproduced by artificially broadening the size distribution of equivalent spheres. This is particularly true for larger real refractive indices. For small real refractive indices, spherical/nonspherical differences are less pronounced (Fig. 7). However, even in this case the differences are big enough to distinguish spherical and nonspherical polarization patterns. We also note that even for very small particles, there are discernable spherical/nonspherical differences; e.g., broader size distributions for spherical particles seem to always compress the Rayleigh region, while increasing nonsphericity appears to expand that region to somewhat larger size parameters (cf. Ref. 11 and 44).

Our calculations also show that polarization patterns for prolate and oblate spheroids of the same aspect ratio are similar despite their very different shapes at larger aspect ratios (Figs. 5–7). In most cases the difference between prolate and oblate spheroids with the same aspect ratio is much smaller than the difference between the spheroids and equivalent spheres. It thus seems that the aspect ratio can serve as a rather general characteristic of particle nonsphericity, at least for convex bodies.

Figures 5 and 6 show that spherical/nonspherical differences are accumulated gradually with increasing particle aspect ratio. Although the polarization diagrams for prolate and oblate spheroids with, e.g., $\epsilon = 1.6$ are already quite different from those for equivalent spheres, there is no sharp cutoff in ϵ below which polarization patterns may be classified as "almost spherical", while above which they are distinctly nonspherical. This conclusion is in full agreement with laboratory measurements by Perry et al,[53] who did not find substantial differences between polarization measured for nearly spherically shaped particles composed of $(NH_4)_2SO_4$ and theoretical Mie calculation for equivalent spheres.

The most prominent polarization feature of nonspherical scattering is a bridge of positive polarization at scattering angles near 120° which extends from the region of Rayleigh scattering (cf. Ref. 10). This bridge is absent for spherical particles with refractive index $1.5 + 0.02i$, but appears for both prolate and oblate spheroids with aspect ratios greater than about 1.6. The bridge is already present for spherical particles with real refractive index 1.3 (Fig. 7), but it becomes wider with increasing aspect ratio. Figure 7 demonstrates that the bridge of positive polarization is a

universal characteristic of spheroidal scattering, although it becomes less pronounced with increasing real part of the refractive index. It is seen that for particles of a given shape, the strength of this polarization feature is a sensitive characteristic of the real refractive index.

The bridge of positive polarization at scattering angles near 120° was also observed by Perry et al[53] in their laboratory polarization measurements for narrow size distributions of nearly cubically shaped NaCl particles with mean size parameters from 3.1 to 19.9. From our extensive calculations and the measurements by Perry et al, it appears that the linear polarization of light scattered by nonspherical particles tends to be positive at middle scattering angles (cf. Ref. 10). If the refractive index of the scattering particles is known a priori, this polarization feature may be very useful in distinguishing between spherical and nonspherical particles based on remote measurements of linear polarization. However, in practice experimental data are often available only for a restricted interval of scattering angles and/or a narrow spectral range. In this case, if the real refractive index is small (e.g., 1.3), it may be difficult to confidently determine the shape of the particles (Fig. 7). It also follows from our calculations displayed in Fig. 7 that if the volume of experimental data is limited, it is easy to misinterpret measurements for nonspherical particles in terms of scattering by spheres having a (much) smaller real refractive index.

The effect of the imaginary part of the refractive index is demonstrated in Fig. 8. One sees that with increasing absorption, the region of positive polarization spreads out, and the difference between spherical and nonspherical particles vanishes. In the limit of sufficiently large absorption, the scattering diagram is of course dominated by the positively polarized light reflected by the particle surface.

3.3. *Effects of concavity*

So far, we have considered only light scattering by spheroidal particles which are convex bodies. However, Zerull[54] and Wiscombe and Mugnai[30] claimed that the effects of particle concavity on the scattering patterns might be rather significant. To examine these effects, one may use the family of Chebyshev particles which can be obtained by continuously deforming a sphere by means of a Chebyshev polynomial of degree n.[3] The shape of a Chebyshev particle in the spherical coordinate system is given by the equation

$$r(\theta, \phi) = r_0[1 + \xi T_n(\cos\theta)], \quad |\xi| < 1, \tag{14}$$

where r_0 is the radius of the unperturbed sphere, ξ is the deformation parameter, and $T_n(\cos\theta) = \cos n\theta$ is the Chebyshev polynomial of degree n. All the Chebyshev particles with $n \geqslant 2$ become partially concave as the absolute value of the deformation parameter ξ increases. Three-dimensional drawings of different Chebyshev particles may be found in Ref. 12.

Since T-matrix computations converge only for modest absolute values of the deformation parameter ξ, our present examination is restricted to scattering by slightly concave particles. Figure 9 shows the results of calculations for Chebyshev particles with $n = 4$, $\xi = \pm 0.1$, $v_{\text{eff}} = 0.03$, and refractive index $1.5 + 0.02i$. Since it is rather difficult to calculate the average projected area for randomly oriented partially concave bodies, we define here the equivalent size of Chebyshev particles as the radius of the equal-surface-area sphere. In Fig. 9, the computations for the Chebyshev particles are compared with calculations for surface-equivalent spheroids with the aspect ratio $\epsilon = 1.3$. This particular aspect ratio was chosen after calculating polarization diagrams for spheroids with the aspect ratio step size $\Delta\epsilon = 0.1$ and selecting the diagrams most similar to those for the Chebyshev particles. Figure 9 shows that for the nearly spherically shaped particles, the polarization diagrams are not dramatically different, and the degree of their departure from the diagrams for the equivalent spheres (Fig. 2) is, generally, the same. We also note that although the shape of the Chebyshev particles with $\xi = +0.1$ and $\xi = -0.1$ is quite different, the corresponding polarization diagrams are more similar to one another than to the diagrams for the surface-equivalent spheroids. The same is true for the prolate and oblate spheroid of the same aspect ratio $\epsilon = 1.3$, thus suggesting that differences between convex and concave particles may be somewhat more noticeable than those due to shape differences for either type of particle. We must, however, emphasize that the absolute value of the deformation parameter $|\xi| = 0.1$ is too small to make definitive conclusions about the general effects of concavity.

4. CONCLUSIONS

In this paper, linear polarization of light scattered by polydisperse, randomly oriented, rotationally symmetric particles was extensively studied. Following Hansen and Travis,[28] we have used as the primary model parameters of a size distribution the effective size parameter and effective variance. Because of some computational limitations, our survey was confined to *effective* equivalent-sphere size parameters less than 15. However, as was noted by Hansen and Travis[28] and Coffeen and Hansen,[1] the region of size parameters extending from the domain of Rayleigh scattering to roughly 15 is especially interesting because here linear polarization is a complicated function of size parameter and cannot be computed by using geometrical optics or Rayleigh approximations. The main body of our computations pertain to convex spheroidal particles. The illustrative calculations for weakly concave Chebyshev particles show that the effects of concavity on the linear polarization may require special attention. Unfortunately, because of computational difficulties, we were not able to make definitive conclusions based on calculations for particles with increasing degree of concavity.

We believe that our survey is a unique source of information about polarizing properties of nonspherical particles because, even after a strong distillation of the available numerical data, it includes calculations for over 150,000 different nonspherical particles in random orientation with monodisperse equivalent-sphere size parameters up to 30. To display our calculations, we used color contour plots of linear polarization as a function of the scattering angle and effective equivalent-sphere size parameter, which is, apparently, the only way of representing the large volume of numerical results in an economical and yet comprehensible way. Based on these extensive calculations, we were able to make several rather general conclusions about the influence of particle size distribution, shape, and refractive index on the polarization patterns of the scattered light and discussed some implications for remote sensing studies. The main results of our analysis can be summarized as follows:

(1) As for spherical particles, broadening the size distribution of randomly oriented nonspherical particles smooths out the interference structure of polarization patterns characteristic for particles of a single size.
(2) One of the effects of particle nonsphericity is also to wash out the interference structure and make linear polarization more neutral. In general, polarization diagrams for nonspherical particles reveal less structure than those for equivalent spheres.
(3) Polarization patterns for nearly spherically shaped particles are close to those for equivalent spheres. For highly aspherical particles, spherical/nonspherical differences are significant and make the Mie theory completely inapplicable.
(4) The most prominent feature of nonspherical scattering is the bridge of positive polarization at scattering angles near 120° which extends from the region of Rayleigh scattering. If the refractive index of scattering particles is a priori known, this polarization feature can be used to distinguish between spherical and nonspherical shapes. For particles of a given shape, the strength of this feature is a sensitive characteristic of the real part of the refractive index.
(5) Polarization patterns for prolate and oblate spheroids of the same aspect ratio are similar, indicating that the aspect ratio may be a relevant shape parameter for convex particles.
(6) The use of the Mie theory to interpret remote polarization measurements for nearly spherically shaped particles may result in an overestimation of the width of the size distribution. For highly irregular particles, the use of the Mie theory may lead to a substantial underestimation of the real part of the refractive index.
(7) Spherical/nonspherical differences in polarization disappear for large values of the imaginary part of the refractive index.

Note that our conclusions are in good agreement with the results of the experimental study by Perry et al.[53]

Finally we emphasize that, beyond our basic conclusions, this survey is also a convincing demonstration of the high efficiency of our numerical method. While Figs. 2–9 represent calculations for over 150,000 different nonspherical particles in random orientation, these computations took less than 300 hours of CPU time on an IBM RISC/6000 Model 37T

workstation. An additional important advantage of this method is that its principal output in the form of expansion coefficients[55–58] can be directly used in radiative transfer calculations.[59–61] As was demonstrated by Wauben et al,[61] particle nonsphericity may strongly affect the polarization of multiply scattered light as well.

Acknowledgements—We are grateful to J. E. Hansen and M. Sato for many useful discussion, W. M. F. Wauben, W. J. Wiscombe, N. V. Voshchinnikov, and an anonymous Reviewer for valuable comments and suggestions, and K. Feng and J. Jonas for programming support. This work was supported in part by the Earth Observing System Project managed by Goddard Space Flight Center in providing for the Earth Observing Scanning Polarimeter instrument analysis and algorithm development.

REFERENCES

1. D. L. Coffeen and J. E. Hansen, in *Planets, Stars and Nebulae Studied with Photopolarimetry*, T. Gehrels ed., pp. 518–581, University of Arizona Press, Tucson, AZ (1974).
2. J. B. Pollack and J. N. Cuzzi, *J. Atmos. Sci.* **37,** 868 (1980).
3. A. Mugnai and W. J. Wiscombe, *J. Atmos. Sci.* **37,** 1291 (1980).
4. T. J. Nevitt and C. F. Bohren, *J. Clim. Appl. Meterorol.* **23,** 1342 (1984).
5. Y. Takano and K.-N. Liou, *J. Atmos. Sci.* **46,** 3 (1989).
6. K. Sassen, *Bull. Am. Meteorol. Soc.* **72,** 1848 (1991).
7. C. Bohren and S. B. Singham, *J. Geophys. Res.* **96,** 5269 (1991).
8. B. Ragent, C. A. Privette, P. Avrin, J. G. Waring, C. E. Carlston, T. C. D. Knight, and J. P. Martin, *Space Sci. Rev.* **60,** 179 (1992).
9. J. E. Penner, R. L. Charlson, J. M. Hales, N. Laulainen, R. Leifer, T. Novakov, J. Ogren, L. F. Radke, S. E. Schwartz, and L. Travis, "Quantifying and Minimizing Uncertainty of Climate Forcing by Anthropogenic Aerosols," Report DOE/NBB-0092T, DOE (1993).
10. S. Asano and M. Sato, *Appl. Opt.* **19,** 962 (1980).
11. F. Kuik, "Single Scattering of Light by Ensembles of Particles with Various Shapes," Ph.D. Thesis, Free University, Amsterdam (1992).
12. W. J. Wiscombe and A. Mugnai, "Single Scattering from Nonspherical Chebyshev Particles: a Compendium of Calculations," NASA Ref. Publ. 1157, NASA/GSFC, Greenbelt, MD (1986); A. Mugnai and W. J. Wiscombe, *Appl. Opt.* **25,** 1235 (1986).
13. S. C. Hill, A. C. Hill, and P. W. Barber, *Appl. Opt.* **23,** 1025 (1984).
14. J. F. de Haan, "Effects of Aerosols on the Brightness and Polarization of Cloudless Planetary Atmospheres," Ph.D. Thesis, Free University, Amsterdam (1987).
15. F. Kuik, J. F. de Haan, and J. W. Hovenier, *JQSRT* **47,** 477 (1992).
16. M. I. Mishchenko, *Astrophys. Space Sci.* **164,** 1 (1990).
17. M. I. Mishchenko, *JOSA A* **8,** 871 (1991); errata **9,** 497 (1992).
18. P. C. Waterman, *Phys. Rev. D* **3,** 825 (1971).
19. P. W. Barber and S. C. Hill, *Light Scattering by Particles: Computational Methods*, World Scientific, Singapore (1990).
20. L. Tsang, J. A. Kong, and R. T. Shin, *Theory of Microwave Remote Sensing*, Wiley–Interscience, New York, NY (1985).
21. M. I. Mishchenko, *Appl. Opt.* **32,** 4652 (1993).
22. M. I. Mishchenko and L. D. Travis, in *Atmospheric Propagation and Remote Sensing II*, A. Kohnle and W. B. Miller eds., Proc. SPIE 1968, pp. 118–129 (1993).
23. W. M. F. Wauben, private communication (1993).
24. J. J. Goodman, B. T. Draine, and P. J. Flatau, *Opt. Lett.* **16,** 1198 (1991).
25. S. Asano and G. Yamamoto, *Appl. Opt.* **14,** 29 (1975).
26. R. W. Schaefer, "Calculations of the Light Scattered by Randomly Oriented Ensembles of Spheroids of Size Comparable to the Wavelength," Ph.D. Thesis, State University of New York, Albany, NY (1980).
27. J. I. Hage, J. M. Greenberg, and R. T. Wang, *Appl. Opt.* **30,** 1141 (1991).
28. J. E. Hansen and L. D. Travis, *Space Sci. Rev.* **16,** 527 (1974).
29. C. F. Bohren and D. R. Huffman, *Adsorption and Scattering of Light by Small Particles*, Wiley, New York, NY (1983).
30. W. J. Wiscombe and A. Mugnai, *Appl. Opt.* **27,** 2405 (1987).
31. J. E. Hansen and J. W. Hovenier, *J. Atmos. Sci.* **31,** 1137 (1974).
32. K. Kawabata, D. L. Coffeen, J. E. Hansen, W. A. Lane, M. Sato, and L. D. Travis, *J. Geophys. Res.* **85,** 8129 (1980).
33. R. Santer, M. Herman., D. Tanré, and J. Lenoble, *J. Geophys. Res.* **93,** 14209 (1988).
34. E. E. Russell, F. G. Brown, R. A. Chandos, W. C. Fincher, L. F. Kubel, A. A. Lacis, and L. D. Travis, *Space Sci. Rev.* **60,** 531 (1992).
35. L. D. Travis, in *Polarization and Remote Sensing*, W. G. Egan ed., Proc. SPIE 1747, pp. 154–164 (1992).
36. J. Hansen, W. Rossow, and I. Fung (Eds.), "Long-Term Monitoring of Global Climate Forcings and Feedbacks," NASA Conf. Publ. 3234, NASA/GSFC, Greenbelt, MD (1993).

37. F. M. Bréon, A. Bricaud, J. C. Buriez, P. Y. Deschamps, J. L. Deuzé, M. Herman, M. Leroy, A. Podaire, and G. Séze, *IEEE Trans. Geosci. Remote Sens.*, submitted (1993).
38. H. C. van de Hulst, *Light Scattering by Small Particles*, Wiley, New York, NY (1957).
39. P. Stammes, "Light Scattering Properties of Aerosols and the Radiation Inside a Planetary Atmosphere," Ph.D. Thesis, Free University, Amsterdam (1989).
40. M. Hofer and O. Glatter, *Appl. Opt.* **28,** 2389 (1989).
41. V. N. Lopatin and F. Ya. Sid'ko, *Introduction to Optics of Cell Suspensions*, Nauka, Novosibirsk (1988).
42. N. V. Voshchinnikov, *Astron. Zh.* **67,** 851 (1990); N. V. Voshchinnikov and V. G. Farafonov, *Astrophys. Space Sci.* **204,** 19 (1993).
43. M. I. Mishchenko, *Astrophys. J.* **367,** 561 (1991).
44. M. I. Mishchenko, *Earth, Moon, Planets* **57,** 203 (1992).
45. N. G. Khlebtsov, A. G. Melnikov, and V. A. Bogatyrev, *J. Colloid Interface Sci.* **146,** 463 (1991).
46. V. Vouk, *Nature* **162,** 330 (1948).
47. A. Lacis, J. Hansen, and M. Sato, *Geophys. Res. Lett.* **19,** 1607 (1992).
48. O. B. Toon and J. B. Pollack, *J. Appl. Meteorol.* **15,** 225 (1976).
49. R. N. Halthore, B. L. Markham, R. A. Ferrare, and T. O. Aro, *J. Geophys. Res.* **97,** 18769 (1992); R. C. Wrigley, M. A. Spanner, R. E. Slye, R. F. Pueschel, and H. R. Aggarwal, *J. Geophys. Res.* **97,** 18797 (1992); J. L. Deuzé, F. M. Bréon, P. Y. Deschamps, C. Devaux, M. Herman, A. Podaire, and J. L. Roujean, *Rem. Sens. Environ.* **45,** 137 (1993).
50. G. A. d'Almeida, P. Koepke, and E. P. Shettle, *Atmospheric Aerosols. Global Climatology and Radiative Characteristics*, Deepak Publishing, Hampton, VA (1991).
51. H. Gerber, *J. Atmos. Sci.* **36,** 2502 (1979).
52. M. Sato, private communication (1992).
53. R. J. Perry, A. J. Hunt, and D. R. Huffman, *Appl. Opt.* **17,** 2700 (1978).
54. R. H. Zerull, *Beitr. Phys. Atmos.* **649,** 168 (1976).
55. H. Domke, *Astrophys. Space Sci.* **29,** 379 (1974).
56. O. I. Bugaenko, *Izv., Atmos. Oceanic Phys.* **12,** 366 (1976).
57. C. E. Siewert, *Astrophys. J.* **245,** 1080 (1981).
58. J. W. Hovenier and C. V. M. van der Mee, *Astron. Astrophys.* **128,** 1 (1983).
59. M. I. Mishchenko, *JQSRT* **46,** 171 (1991).
60. W. M. F. Wauben and J. W. Hovenier, *JQSRT* **47,** 491 (1992).
61. W. M. F. Wauben, J. F. de Haan, and J. W. Hovenier, *JQSRT* **50,** 237 (1993).